Numerical Methods for Density Variation Fluid Flow Analysis (Evolution Equations and Asymptotic Analysis of Solutions)

AUTHOR(S):

Arima, Toshiyuki

CITATION:

Arima, Toshiyuki. Numerical Methods for Density Variation Fluid Flow Analysis (Evolution Equations and Asymptotic Analysis of Solutions). 数理解析研究所講究録 2005, 1436: 187-211

ISSUE DATE:

2005-06

URL:

http://hdl.handle.net/2433/47460

数理解析研究所講究録 1436 巻 2005 年 187-211

Numerical Methods for Density Variation Fluid Flow Analysis

本田技術研究所 和光基礎技術研究センター 有馬敏幸 (Toshiyuki Arima)
Wako Research Center, Honda R&D Co., Ltd.

1 Introduction

Mathematical models which describe environmental fluid flow motions are discussed, and numerical methods for environmental fluid flow analysis are treated, while paying attention on the grade of density change which is one of the most important factors of environmental fluids. In this paper, the starting point is to present a statement of a complete system of detailed governing equations for fluid flows involving chemical reactions. Then, an approximate mathematical model is formulated in terms of rate of density variation and stable numerical schemes for the approximate model are proposed and verified in a numerical way.

This paper is organized as follows: In Section 2, a complete system of detailed governing equations for fluid flows involving chemical reactions is presented. In Section 3, so-called *Boussinesq approximations* are employed in the full Navier-Stokes equations to construct a mathematical model describing fluid flow fields in the case in which the ratio of change in density to the change in temperature is relatively small. A new numerical method is proposed that is based on an iterative implicit time evolution and a high-accurate spatial discretization with TVD properties. Numerical simulations of the fluid flow motions around two circular cylinders with ends have been performed as specific fluid flow simulations around structures in environmental fluids by means of our numerical methods.

In Section 4, the low-Mach number approximations are applied to the full Navier-Stokes equations, so that we may construct another type of mathematical models to describe the fluid flow fields in which large variation of density is caused by the large change in temperature. Under the assumption that acoustic effects can be weak relative to advection effects, acoustic effects can be removed from the governing equations. Since the model with low-Mach number approximations includes a model for the incompressible flow and Boussinesq approximations as portions of this model, it is applicable to various problems on environmental fluids with density variation. The iterative implicit scheme proposed in Section 3 is employed for solving this model. Our scheme is verified for test problems which are formulated for flows with large variation of density due to large change in temperature which is caused by chemical reactions.

In Section 5, numerical schemes for solving fully compressible Navier-Stokes equations are discussed, which describe the fluid flow fields in which density variation is caused by not only change in temperature but also by variation of pressure. Although the acoustic effect can be investigated through the full Navier-Stokes equations, classical numerical schemes seems to be difficult to treat the flow fields in the case where the Mach number is less than 0.1. This difficulty is caused by a disparity between the advection velocity and sound speed which correspond to the

eigenvalues of the system. This lead us to stiffness problem for the system and hence the round-off errors make the algebraic problem ill-conditioned under the low Mach number approximations. A new numerical scheme is proposed to overcome this difficulty, in order to make it possible to perform numerical analysis for low-speed flows up to high-speed flows. An important feature of our scheme is that dependent variables of the governing equations maintain the conservative variables through the preconditioning method to compress the eigenvalues of the system. Since the conservative form are usually used in the numerical schemes for the compressible flows in order to get the solutions including shock waves (discontinuities), our method enables us to change the code for the compressible case to a unified version.

2 Governing Equations

The starting point of our argument is to formulate the governing equations for the fluid phenomena under consideration. In this section, a complete system of governing equations for fluid flows involving chemical reactions are first presented.

2.1 Conservative form of equations for reacting flows

Equations describing chemically reactive flows with N participating species in conservative formulation are stated as follows:

- Mass Conservation for Chemical Species:

$$\frac{\partial \rho Y_i}{\partial t} + \nabla \cdot (\rho Y_i \boldsymbol{v}) = -\nabla \cdot \boldsymbol{j}_i + w_i \qquad (i = 1, 2, ...N) \tag{1}$$

- Mass Conservation for Mixture Gases:

$$\frac{\partial \rho}{\partial t} + \nabla \cdot (\rho \boldsymbol{v}) = 0 \tag{2}$$

- Conservation of Momentum:

$$\frac{\partial \rho \boldsymbol{v}}{\partial t} + \nabla \cdot (\rho \boldsymbol{v} \otimes \boldsymbol{v}) = -\nabla p + \nabla \cdot \boldsymbol{\tau} + \rho \sum_i^N Y_i \boldsymbol{f}_i \tag{3}$$

- Conservation of Energy

$$\rho \frac{\partial \rho e_t}{\partial t} + \nabla \cdot \{(\rho e_t + p)\boldsymbol{v}\} = -\nabla \cdot \boldsymbol{q} + \nabla \cdot (\boldsymbol{\tau} \cdot \boldsymbol{v}) + \rho \sum_i^N Y_i \boldsymbol{f}_i \cdot \boldsymbol{v} + \sum_i^N \boldsymbol{f}_i \cdot \boldsymbol{j}_i \tag{4}$$

$$e_t = h - \frac{p}{\rho} + \frac{1}{2}\boldsymbol{v} \cdot \boldsymbol{v} \tag{5}$$

- Thermodynamic Equation of State:

$$p = \rho R T M^{-1}, \quad M = \left(\sum_{i=1}^N Y_i / M_i \right)^{-1}, \tag{6}$$

where ρ means the density, $\boldsymbol{v}$ denotes the velocity vector, p stands for the pressure, $\boldsymbol{\tau}$ represents the viscous tensor, $\boldsymbol{f}_i$ means the body force per unit mass of species i, Y_i represents the mass fraction of chemical species i, $\boldsymbol{j}_i$ denotes the diffusive flux vector of species i, w_i stands for the mass production rate of species i, e_t is the total energy, $\boldsymbol{q}$ denotes the heat flux vector, h represents the enthalpy, R is the universal gas constant, T denotes the temperature, M means the mean molecular mass, and M_i stands for the molecular mass of species i. The viscous stress tensor $\boldsymbol{\tau}$, the diffusive flux vector of species $\boldsymbol{j}_i$, and the heat flux vector $\boldsymbol{q}$ will be given in the section of "Constitutive equation".

To be consistent with mass conservation, the species mass fractions, the diffusion velocities and chemical sources must satisfy

$$\sum_i^N Y_i = 1, \quad 0 \le Y_i \le 1, \quad \sum_i^N \boldsymbol{j}_i = 0, \quad \sum_i^N w_i = 0 \tag{7}$$

Note that summation of conservations equations for all species in (1) implies total mass conservation, (2), so that one of those $N+1$ equations is redundant.

2.2 Constitutive equations

The viscous stress tensor, diffusive flux vector, and heat flux vector are modeled by means of the following constitution equations:

- **Viscous stress tensor**

$$\boldsymbol{\tau} = \mu \left\{ \left(\nabla \boldsymbol{v} + (\nabla \boldsymbol{v})^T \right) - \frac{2}{3} (\nabla \cdot \boldsymbol{v}) \boldsymbol{I} \right\} \tag{8}$$

The viscous coefficient μ is obtained by semi-empirical formulae due to Wilke[11] and modified by Bird, et al[1].

- **Diffusive flux vector of species**

$$\boldsymbol{j}_i = \rho \boldsymbol{V}_i Y_i \tag{9}$$

where $\boldsymbol{V}_i$ denotes the diffusion velocity of species i. In this paper a form of Fick's law form is employed to evaluate the diffusion velocities of the species in the associated mass-diffusion processes by introducing a diffusion coefficient D_i.

$$\boldsymbol{V}_i = -D_i Y_i^{-1} \nabla Y_i \tag{10}$$

The diffusion coefficients D_i are modeled in terms of the binary diffusion coefficient matrix D_{ij} [1]. It turns out that the diffusive flux vector may be modeled as

$$\boldsymbol{j}_i = -\rho D_i \nabla Y_i, \tag{11}$$

- **Thermal flux vector**

Dufour effect and thermal radiation are neglected in the present discussions. Hence we have

$$\boldsymbol{q} = -\lambda \nabla T + \sum_{i}^{N} h_i \boldsymbol{j}_i \tag{12}$$

where λ denotes heat conductivity. The coefficient of heat conductivity of the mixture is obtained through a combination averaging formula [1].

2.3 A model of Chemical reactions

The parameter w_i in the governing equations represents the rate of mass production of species i. In order to evaluate this, we need an appropriate model of chemical reactions. Elementary chemical reactions are described as

$$\sum_{i=1}^{N} \nu_i^{'} m_i \underset{k_b}{\overset{k_f}{\rightleftharpoons}} \sum_{i}^{N} \nu_i^{''} m_i, \tag{13}$$

where $\nu_i^{'}$s are stoichiometric coefficients of reactions for educts, $\nu_i^{''}$s are stoichiometric coefficients of reactions for products, m_is are the names of the species i, k_f stands for reaction rate of forward reaction, and k_b means a reaction rate for the backward reaction. The mass production rate w_i for species i is computed through the following equation:

$$w_i = M_i \sum_{k=1}^{Nr} \left(\nu_{i,k}^{''} - \nu_{i,k}^{'} \right) \dot{w}_k, \tag{14}$$

where M_i denotes the molecular mass of species i, N_r means the total number of elementary chemical reaction stages. The symbol $\dot{w}_k$ denotes the progress rate of the k-th stage of the elementary chemical reaction, and it is calculated as follows:

$$\dot{w}_k = k_{f,k} \prod_{i}^{N} C_i^{\nu_{i,k}^{'}} - k_{b,k} \prod_{i}^{N} C_i^{\nu_{i,k}^{''}} \tag{15}$$

where $k_{f,k}$ represents the reaction rate coefficient for forward reaction of the k-th stage of the elementary reaction, $k_{b,k}$ is the coefficient of reaction rate for backward reaction of the k-th stage of the elementary reaction, and C_i is the concentration of species i, that is defined as $C_i = Y_i \rho / M_i$. The reaction rate coefficients $k_{f,k}$ and $k_{b,k}$ for the k-th elementary reaction are given, respectively, by the Arrhenius-law.

$$k_{f,k} = B_{f,k} T^{\alpha_{f,k}} exp\left(-\frac{E_{f,k}}{RT} \right), \tag{16}$$

$$k_{b,k} = B_{b,k} T^{\alpha_{b,k}} exp\left(-\frac{E_{b,k}}{RT} \right), \tag{17}$$

where the parameters $B_{f,k}$ and $B_{b,k}$ are frequency factors, $\alpha_{f,k}$ and $\alpha_{b,k}$ are temperature indices, and $E_{f,k}$ and $E_{b,k}$ are activation energies of the forward and backward reactions, respectively. This law is empirically validated, while the constants are usually determined by experiments.

3 Numerical Simulations with Boussinesq Approximations

A numerical model of fluid motions is derived from the continuous model by applying the Boussinesq approximation to the Navier-Stokes equations, in the form of fully implicit discretization in time. For discretization of nonlinear convection terms, an upwind difference of the third-order accuracy or a TVD scheme of the third-order accuracy is used to suppress the dispersion errors that are caused by finite-difference approximation. The finite-difference schemes obtained as nonlinear algebraic equations are numerically solved by Newton-Raphson's iteration method. The results of numerical simulations for the fluid motions around two circular cylinders with ends are exhibited in terms of environmental fluid.

3.1 A mathematical model of environmental fluids

We apply the Boussinesq approximation to the Navier-Stokes system and formulate the following system of Equations (18-20) as our mathematical model for describing the motion of environmental fluid:

$$\nabla \cdot \boldsymbol{v} = 0 \tag{18}$$

$$\rho\left[\frac{\partial \boldsymbol{v}}{\partial t} + (\boldsymbol{v}\cdot\nabla)\boldsymbol{v}\right] = -\nabla p + \mu\Delta\boldsymbol{v} - \rho\beta(T - T_0)\boldsymbol{g} \tag{19}$$

$$\rho C_p\left[\frac{\partial T}{\partial t} + (\boldsymbol{v}\cdot\nabla)T\right] = \kappa\Delta T + S_c \tag{20}$$

Here the parameters $\boldsymbol{v}$, ρ, p, μ, β, $\boldsymbol{g}$, T and C_p represent the velocity vector, density, pressure, viscosity coefficient, rate of volume expansion, the acceleration of gravity, temperature and the specific heat at constant pressure, respectively. Also, the coefficient κ means the thermal conductivity and S_c stands for the sum of heat sources in the fluid. In this study, ρ, μ, C_p, and κ are supposed to be fixed values that are specified at a state of hydrostatic equilibrium. Our main objective here is to obtain numerical data describing the flow field around bodies in an environmental fluid under consideration. For this purpose we impose the following boundary conditions:

(B1) On the inflow boundary $\partial\Omega_i$ with outward normal vector $\boldsymbol{n}_i = \boldsymbol{n}_i(\hat{\boldsymbol{x}})$, we impose Dirichlet boundary conditions for $\boldsymbol{v}$ and T and homogeneous Neumann boundary conditions for p:

$$\boldsymbol{v}(\hat{\boldsymbol{x}},t) = \boldsymbol{v}_{\partial\Omega_i}(t),\quad T(\hat{\boldsymbol{x}},t) = T_{\partial\Omega_{in}}(t),\quad \frac{p(\hat{\boldsymbol{x}},t)}{\partial n_i} = 0,\quad \hat{\boldsymbol{x}}\in\partial\Omega_i \tag{21}$$

(B2) On the outflow boundary $\partial\Omega_o$ with outward normal vector $\boldsymbol{n}_o = \boldsymbol{n}_o(\hat{\boldsymbol{x}})$, we impose homogeneous Neumann boundary conditions for $\boldsymbol{v}$, T and Dirichlet boundary conditions for p:

$$\frac{\boldsymbol{v}(\hat{\boldsymbol{x}},t)}{\partial n_o} = 0,\quad \frac{T(\hat{\boldsymbol{x}},t)}{\partial n_o} = 0,\quad p(\hat{\boldsymbol{x}},t) = p_{\partial\Omega_o}(t),\quad \hat{\boldsymbol{x}}\in\partial\Omega_o \tag{22}$$

(B3) On the surface of each body standing in the fluid, Ω_s with outward normal vector $\boldsymbol{n}_s = \boldsymbol{n}_s(\hat{\boldsymbol{x}})$, we impose the non-slip condition for $\boldsymbol{v}$ and homogeneous Neumann boundary conditions for T. We also impose an inhomogeneous Neumann boundary conditions for p which is obtained from Equation (19) in the normal direction to the surface:

$$\boldsymbol{v}(\hat{\boldsymbol{x}},t) = 0, \quad \frac{T(\hat{\boldsymbol{x}},t)}{\partial n_s} = 0, \quad \frac{p(\hat{\boldsymbol{x}},t)}{\partial n_s} = \mu(\boldsymbol{n}_s \cdot \Delta \boldsymbol{v}(\hat{\boldsymbol{x}},t)) - \rho\beta(T(\hat{\boldsymbol{x}},t) - T_0)(\boldsymbol{n}_s \cdot \boldsymbol{g}), \quad \hat{\boldsymbol{x}} \in \partial\Omega_s \tag{23}$$

It is a characteristic feature of this paper that a new numerical scheme for the continuous model mentioned above is proposed in such a way that a fully implicit scheme is employed.

3.2 Numerical Methods

Since the governing equations under the Boussinesq approximation are of the forms similar to the incompressible Navier-Stokes equations, the numerical methods which have been developed for the incompressible Navier-Stokes equations, e.g., MAC method (marker and cell method) [5] may be applicable. In this paper, we apply the iterative method such that the MAC method is rephrased in terms of fully implicit procedure.

3.2.1 A mathematical model of numerical fluids

Making discretization in time in Equations (18)-(20) by use of the Euler implicit method, we obtain the following system of equations:

$$\nabla \cdot \boldsymbol{v}^{n+1} = 0 \tag{24}$$

$$\frac{\boldsymbol{v}^{n+1} - \boldsymbol{v}^n}{\Delta t} = -(\boldsymbol{v}^{n+1} \cdot \nabla)\boldsymbol{v}^{n+1} - \frac{1}{\rho}\boldsymbol{\nabla} p^{n+1} + \frac{\mu}{\rho}\Delta \boldsymbol{v}^{n+1} - \beta(T^{n+1} - T_0)\boldsymbol{g} \tag{25}$$

$$\frac{T^{n+1} - T^n}{\Delta t} = -(\boldsymbol{v}^{n+1} \cdot \nabla)T^{n+1} + \frac{1}{\rho C_p}\kappa \Delta T^{n+1} + \frac{Sc}{C_p \rho} \tag{26}$$

Substituting Equation (25) into Equation (24), Poisson's equation for pressure is derived:

$$\boldsymbol{\Delta} p^{n+1} = -\rho \left[\nabla \cdot \left\{ (\boldsymbol{v}^{n+1} \cdot \boldsymbol{\nabla})\boldsymbol{v}^{n+1} \right\} - \frac{\nabla \cdot \boldsymbol{v}^n}{\Delta t} \right] - \rho\beta \nabla \cdot (T^{n+1}\boldsymbol{g}). \tag{27}$$

In what follows, we regard Equations (25), (26) and (27) as the governing equations for the motion of numerical fluids. Our main objective here is to investigate the numerical solvability of this basic model.

3.3 Iterative implicit scheme

Our mathematical models of the numerical fluid as expressed by Equations (25), (26) and (27) are fully implicit in time and this implicit form guarantees numerical stability and robustness. We adopt a procedure of constructing iterative numerical solutions that is not only much more economical but also remains most of the stability and accuracy properties of the fully implicit scheme. The iteration procedure employed in the present study is summarized as follows: In the

following, the superscript n refers to the value which are known from the previous time step, the superscript k refers to the iteration cycle between the solutions at time step n and $n+1$, the superscript 0 is associated with an initial guess for the first iteration step $k=0$.

Step1: Choose an inferred initial data for computing the values $\boldsymbol{v}^{n+1}$, p^{n+1}, and T^{n+1} at the next time step. The simplest choice is to use the solutions themselves at the current time step:

$$\boldsymbol{v}^0 = \boldsymbol{v}^n, \quad p^0 = p^n, \quad T^0 = T^n$$

Step2: Poisson's equation for the pressure (27) is solved by applying the successive over relaxation (SOR) method to get the pressure at the current iteration step, say k:

$$\boldsymbol{\Delta} p^k = -\rho \left[\nabla \cdot \left\{ (\boldsymbol{v}^k \cdot \nabla) \boldsymbol{v}^k \right\} - \frac{\nabla \cdot \boldsymbol{v}^n}{\Delta t} \right] - \rho\beta \nabla \cdot (T^k \boldsymbol{g}) \tag{28}$$

Step3: The following equation of the delta-form for $\delta \boldsymbol{v}^k \, (= \boldsymbol{v}^{k+1} - \boldsymbol{v}^k)$ is solved.

$$\left[1 + \Delta t \left(\boldsymbol{v}^n \cdot \nabla - \frac{\mu}{\rho} \Delta \right) \right] \delta \boldsymbol{v}^k = rhs_m^k, \tag{29}$$

where

$$rhs_m^k = -(\boldsymbol{v}^k - \boldsymbol{v}^n) + \Delta t \left[-(\boldsymbol{v}^k \cdot \nabla) \boldsymbol{v}^k - \frac{1}{\rho} \nabla p^k + \frac{\mu}{\rho} \Delta \boldsymbol{v}^k - \beta (T^k - T_0) \boldsymbol{g} \right]. \tag{30}$$

Step4: Compute the velocity at the next iteration step $k+1$ by

$$\boldsymbol{v}^{k+1} = \boldsymbol{v}^k + \delta \boldsymbol{v}^k. \tag{31}$$

Step5: The following equation of the delta-form for $\delta T^k \, (= T^{k+1} - T^k)$ is solved.

$$\left[1 + \Delta t \left(\boldsymbol{v}^{k+1} \cdot \nabla - \frac{\kappa}{C_p \rho} \Delta \right) \right] \delta T^k = rhs_T^k, \tag{32}$$

where

$$rhs_T^k = -(T^k - T^n) + \Delta t \left[-(\boldsymbol{v}^{k+1} \cdot \nabla) T^k + \frac{\kappa}{C_p \rho} \Delta T^k + \frac{Sc}{\rho C_p} \right]. \tag{33}$$

Step6: Compute the temperature at the next iteration step $k+1$ by

$$T^{k+1} = T^k + \delta T^k. \tag{34}$$

Step7: Check the convergence of Newton's iteration for the equations of the delta form for the velocity and the temperature as follows:

$$\sum_{\Omega} |\boldsymbol{v}^{k+1} - \boldsymbol{v}^k| < \epsilon_v$$

and

$$\sum_{\Omega} |T^{k+1} - T^k| < \epsilon_T.$$

where $\sum_{\Omega}$ means the summation over the whole computational domain, ϵ_v and ϵ_T are small values prescribed as admissible error bounds which also stand for radii of convergence for the

respective inequalities. This completes one cycle of the iterative process. If more iterations are required, the process should be continued from Step 2. In particular, experiences suggest that only 2 or 3 iterations are enough to get desired approximate numerical solutions.

We find in this scheme that if $|\boldsymbol{v}^{k+1}-\boldsymbol{v}^{k}| \longrightarrow 0$ and $|T^{k+1}-T^{k}| \longrightarrow 0$ then $\boldsymbol{v}^{k}=\boldsymbol{v}^{k+1}=\boldsymbol{v}^{n+1}$, $T^{k}=T^{k+1}=T^{n+1}$ and $p^{k}=p^{n+1}$, because Equations (29) and (32) converge to Equations (25) and (26), respectively, for $\delta\boldsymbol{v}^{k}=0$ and $\delta T^{k}=0$; and then pressure equation (28) converges to Equation (27).

3.4 Spatial discretization

For simplicity, we consider the following time-dependent Cauchy problem in one space dimension

$$\begin{aligned} \frac{\partial\phi}{\partial t}+v\frac{\partial\phi}{\partial x} &= 0, \quad -\infty<x<\infty,\ t\geq 0, \\ \phi(x,0) &= \phi_0(x). \end{aligned} \tag{35}$$

Here $\phi : \mathbb{R}\times\mathbb{R}\rightarrow\mathbb{R}$ means velocity. We find that the solution of this equation has a TVD property because the solution of ϕ of Equation (36) is constant along curve $dx/dt=v$, which is known as the characteristics equation. This can be confirmed by differentiating $\phi(x,t)$ along the curve to find the rate of change of ϕ along the characteristics:

$$\begin{aligned} \frac{d}{dt}\phi(x(t),t) &= \frac{\partial}{\partial t}\phi(x(t),t)+\frac{\partial}{\partial x}\phi(x(t),t)x'(t) \\ &= \phi_t+v\phi_x \\ &= 0. \end{aligned} \tag{36}$$

Therefore, it is possible to construct a TVD scheme by starting with Equation (36). Thus, we consider the following equation similar to Equation (36).

$$\frac{\partial\phi}{\partial t}+\frac{\partial(v\phi)}{\partial x}-\phi\frac{\partial v}{\partial x}=0. \tag{37}$$

Since the form of the second term in the above equation is of the form of derivative of flux, we incorporate a discretization with TVD property, that will be introduced next.

We discretize the $x-t$ plane by choosing a mesh width $h\equiv\Delta x$ and a time step $k\equiv\Delta t$, and define the discrete mesh points (x_i,t_n) by

$$\begin{aligned} x_i &= i\Delta x, \quad i=...,-1,0,1,2,... \\ t_n &= n\Delta t, \quad n=0,1,2,... \end{aligned} \tag{38}$$

It will also be useful to define

$$x_{i+1/2}=x_i+\frac{1}{2}\Delta x=\left(i+\frac{1}{2}\right)\Delta x. \tag{39}$$

For simplicity we take a uniform mesh, with h and k being constant. The finite difference methods we here discuss provide approximations $u_i^n \in \mathbb{R}$ to solution $u(x_i, t_n)$ at the discrete grid points. Here we discretize Equation (35) as follows:

$$\frac{\phi_i^{n+1} - \phi_i^n}{\Delta t} = -\frac{1}{\Delta x}\left(\tilde{f}_{i+\frac{1}{2}} - \tilde{f}_{i-\frac{1}{2}}\right) \tag{40}$$

$\tilde{f}_{1\pm\frac{1}{2}}$ denotes a numerical flux function on the cell interface $x_{i+\frac{1}{2}}$. This can be evaluated as the sum of discretizations of the last term of Equation (37) and the discretized flux of the second term by the Monotone Upstream Centered Schemes for Conservation Laws (MUSCL) method [9] with *minmod* limiter function (see [3]). Since the last term can be discretized as,

$$\phi\frac{\partial v}{\partial x} \Rightarrow \left[(a_{i+\frac{1}{2}} - a_{i-\frac{1}{2}})/\Delta x\right]\phi, \tag{41}$$

with $a = v^n$, the total numerical flux can be evaluated as follows:

$$\begin{aligned}\tilde{f}_{i+\frac{1}{2}} &= -a_{i+\frac{1}{2}}\phi_i + f_{i+\frac{1}{2}}^{(upw)} \\ &+ a_{i+\frac{1}{2}}^{+} \cdot \frac{1}{4}\left[(1+\kappa)\Phi_{i+\frac{1}{2}}^{+C} + (1-\kappa)\Phi_{i+\frac{1}{2}}^{+U}\right] \\ &- a_{i+\frac{1}{2}}^{-} \cdot \frac{1}{4}\left[(1+\kappa)\Phi_{i+\frac{1}{2}}^{-C} + (1-\kappa)\Phi_{i+\frac{1}{2}}^{-U}\right]\end{aligned} \tag{42}$$

The first term of Equation (42) corresponds to the last term of Equation (37). The second term of Equation (47), $f_{i+\frac{1}{2}}^{(upw)}$ corresponds to the first-order accurate upwind difference of the second term of Equation (37) and the other terms are corrections to make the scheme of higher order accuracy. These can be written as follows:

$$f_{i+\frac{1}{2}}^{(upw)} = a_{i+\frac{1}{2}}^{+}\phi_i + a_{i+\frac{1}{2}}^{-}\phi_{i+1}. \tag{43}$$

Here

$$a = v^n, \quad a^{\pm} = v^{\pm} = \frac{1}{2}\left(v^n \pm |v^n|\right), \tag{44}$$

and Φ is defined as follows:

$$\begin{aligned}\Phi_{i+\frac{1}{2}}^{+C} &= minmod\left[\phi_{i+1} - \phi_i, \beta(\phi_i - \phi_{i-1})\right] \\ \Phi_{i+\frac{1}{2}}^{+U} &= minmod\left[\phi_i - \phi_{i-1}, \beta(\phi_{i+1} - \phi_i)\right] \\ \Phi_{i+\frac{1}{2}}^{-C} &= minmod\left[\phi_{i+1} - \phi_i, \beta(\phi_{i+2} - \phi_{i+1})\right] \\ \Phi_{i+\frac{1}{2}}^{-U} &= minmod\left[\phi_{i+2} - \phi_{i+1}, \beta(\phi_{i+1} - \phi_i)\right],\end{aligned} \tag{45}$$

where

$$minmod(x, y) = \frac{1}{2}\left[sgn(x) + sgn(y)\right] min(|x|, |y|), \tag{46}$$

and the parameter β is called a compression parameter in the paper of Chakravarthy [3] and must satisfy $\beta \geq 1$, and its upper bound is determined by the TVD condition. The parameter κ is one for discretization accuracy, e.g., the second-order accuracy for $\kappa = -1$ and $\kappa = 1/3$ for the third-order accuracy, we have $-1 \leq \kappa \leq 1$. The numerical flux $\tilde{f}_{i-\frac{1}{2}}$ is obtained by replacing subscript $i+\frac{1}{2}$ by $i-\frac{1}{2}$. In this replacement of subscripts, we should note that the first term with the replaced subscript is not $-a_{i-\frac{1}{2}}\phi_{i-1}$ but $-a_{i-\frac{1}{2}}\phi_i$. Using $a = a^+ + a^-$, Equation (47) can be rewritten as follows:

$$\begin{aligned}\tilde{f}_{i+\frac{1}{2}} &= a^-_{i+\frac{1}{2}}(\phi_{i+1} - \phi_i) \\ &+ a^+_{i+\frac{1}{2}} \cdot \frac{1}{4}\left[(1+\kappa)\Phi^{+C}_{i+\frac{1}{2}} + (1-\kappa)\Phi^{+U}_{i+\frac{1}{2}}\right] \\ &- a^-_{i+\frac{1}{2}} \cdot \frac{1}{4}\left[(1+\kappa)\Phi^{-C}_{i+\frac{1}{2}} + (1-\kappa)\Phi^{-U}_{i+\frac{1}{2}}\right]\end{aligned} \tag{47}$$

When this scheme is written as

$$u_i^{n+1} = u_i^n - C_{i-\frac{1}{2}}(u_i - u_{i-1}) + D_{i+\frac{1}{2}}(u_{i+1} - u_i), \tag{48}$$

the conditions for this scheme to be a Total Variation Diminishing (TVD) are:

$$C_{i+\frac{1}{1}2} \geq 0, \quad D_{i+\frac{1}{2}} \geq 0, \quad C_{i+\frac{1}{2}} + D_{i+\frac{1}{2}} \leq 1. \tag{49}$$

From the conditions $C_{i+\frac{1}{1}2} \geq 0$ and $D_{i+\frac{1}{2}} \geq 0$, we obtain

$$(1 \leq)\,\beta \leq \frac{3-\kappa}{1-\kappa}. \tag{50}$$

From the conditions $C_{i+\frac{1}{2}} + D_{i+\frac{1}{2}} \leq 1$, we obtain

$$\Delta t \leq \frac{\Delta x}{|a_{i+\frac{1}{2}}| + \frac{1}{4}(a^+_{i+\frac{3}{2}} - a^+_{i-\frac{1}{2}})(\beta(1+\kappa)+1-\kappa)} \tag{51}$$

Under these conditions, the scheme becomes a Total Variation Diminishing (TVD) scheme [6] for the discretization of Equation(40). When the advection speed is constant ($a = const$), it becomes

$$\Delta t \leq \frac{4}{5-\kappa+\beta(1+\kappa)} \cdot \frac{\Delta x}{|a|}. \tag{52}$$

This scheme is of the third-order accuracy for the values $\kappa = \frac{1}{3}$ and $\beta = 4$.

We can directly incorporate this formula with the convective terms on the right-hand side of Equations (30) and (33). Thus, we can easily employ the TVD discretization in our iterative implicit scheme.

3.5 Application to an Environmental Fluid

3.5.1 Settings of numerical simulation

We here discuss flow analysis around cylinders with bottom ends standing in an environmental fluid. In the numerical simulations we have performed, flow analysis was made for a typical fluid flow. Our setting may be outlined as follows: We consider a parallelepiped region $\mathbf{R}$ in $\mathbb{R}^3$ and assume that one side is the inflow boundary and the opposite side is the outflow boundary. We then insert two circular cylinders with radius 1R and length 20R both of which have bottom ends in the region $\mathbf{R}$ in such a way that they are arranged in a row at an interval of 10R and perpendicular to the top side of $\mathbf{R}$, as illustrated in Fig. 1. For convenience, we call the cylinder facing the inflow boundary the front cylinder and the cylinder facing the outflow boundary the rear cylinder. In this setting we performed numerical simulations and made detailed analysis around the two cylinders parallel to each other. Numerical conditions are put in the following

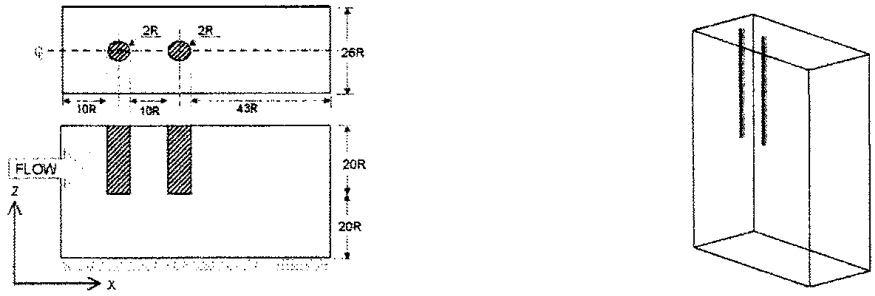

(a) Settings of computational domain (b) 3D view of computational domain

Figure 1: Setting of numerical simulations

way: The Reynolds number ($= \rho|v|2R/\mu$) in accordance with the main flow velocity is assumed to be $Re = 2500$ and the temperature distribution is assumed to follow a linear distribution such that $T = 300K$ on the top of the front cylinder and $T = 290K$ under the bottom end.

3.5.2 Results of numerical simulations

Computation is started with a uniform initial data and qualitative features are investigated by analyzing the numerical results of the simulation at a time step at which the flow field is well developed and reaches a quasi-stationary state. Figure 2 depicts the velocity vector field and contours of the pressure on the cross section containing the axes of the two cylinders. In the velocity vector field upward flows along the back of the front cylinder are observed. These upward flows take place when the horizontal uniform flow runs around the bottom end and are remarkable in a neighborhood of the bottom end and even reach the top part of the cylinder. Similar upward flows are also observed behind the rear cylinder. These flows are formed in such a way that they seem to roll the bottom part up and go up towards the top part. Moreover, such upward flows are observed in a wide range behind the rear cylinder since there are no obstacles. In the figure

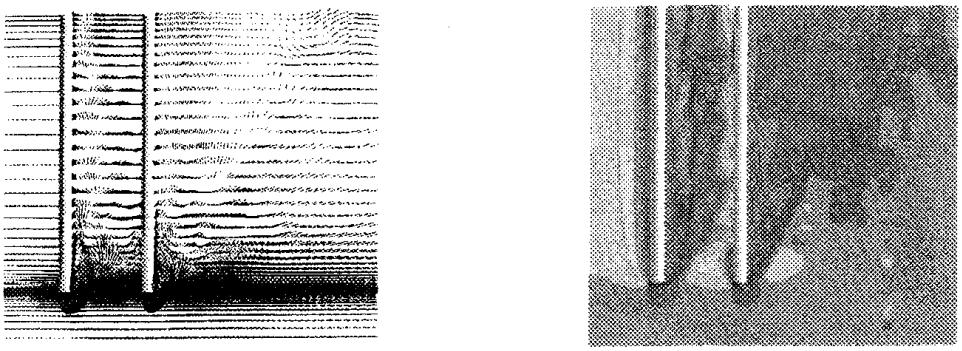

(a) Velocity vector (b) Pressure contour

Figure 2: Computational results on the x-z plane across circular cylinders

of contours of the pressure it is observed that a vertical sequence of separate regions like cells of negative pressure are formed. This is due to the presence of nonstationary vortices of Karman-type. On the other hand, a vertical sequence of regions of positive pressure are observed in the front of the rear cylinder. This phenomenon suggests that the nonstationary vortices generated by the front cylinder interact the regions of stagnation existing in the front of the rear cylinder and deteriorate the stagnation pressure. In Fig. 3 the stream lines and trajectories of particles

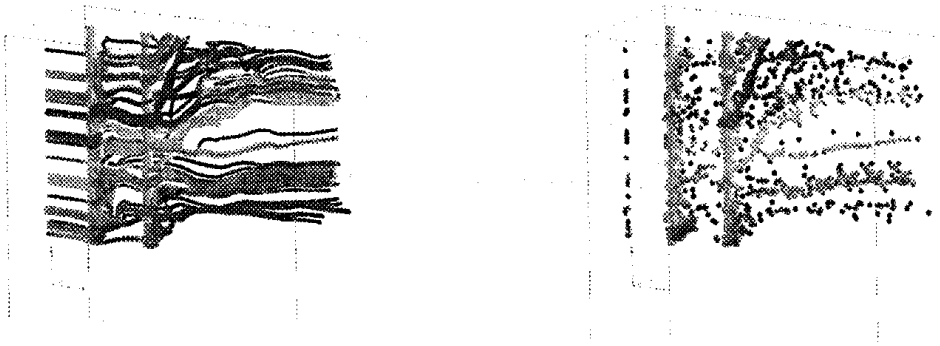

(a) streamlines (b) Particle trajectories

Figure 3: Upward flow motions observed behind two circular cylinders

in the fluid are depicted. Trajectories of particles are drawn in the following way: We release the particles from the back of each cylinder and trace the trajectories forward and backward in time until the particles reach the boundaries of the computational domain and those of the bodies in the fluid. It is seen from Fig. 3(a) that upward flows behind the cylinders are rolling up towards the top. Furthermore, the motion of longitudinal vortices around the bottom sides can be observed as inferred from the iso-surfaces of vorticity. Figure 3(b) is obtained by arranging particles on the same trajectories as in Fig. 3(a) at regular time intervals. From this it is seen that the particle distribution represents how long a particle stay in the flow, and that particles

are concentrated in the back of the front cylinder. These results of numerical simulations may have applications to various environmental problems. It is then expected that new environmental restoration technology will be developed by applying the results of numerical simulations for environmental fluids.

4 Numerical Simulations with Low Mach Number Approximations

A mathematical model of environmental fluid is presented to describe fluid flow motions with large density variations. Moremover the associated numerical methods are discussed. The model of environmental fluid is formulated as a unsteady low-Mach number flow based on the compressible Navier-Stokes equations. For low-Mach number flows, the acoustic effects are assumed to be weak relative to the advection effects. Under this assumption, detailed acoustic effects can be removed from governing equations. The low-Mach number formulation thus enables numerical flow analysis with a projection methodology that uses high-order accurate upwind difference of the convection terms with a time step restricted solely by an advection Courant-Friedrichs-Lewy (CFL) condition. The algorithm presented here is based on an iterative implicit time evolution of second order accuracy and a high-accurate spatial discretization with TVD properties for unsteady low-Mach number flows. It is seen from the results on the verification for test cases of flows with a wide range of density variations that our numerical method is validated.

4.1 Navier-Stokes equations for low Mach numbers

For the Navier-Stokes equations for reactive flows such that density varies in space due to spatial gradients of temperature and mean molecular mass, a similar low-Mach-number approximation can be employed in order to obtain a well-conditioned system. According to Majda [7], the pressure p is split into two parts,

$$p(x,t) = P_{th}(t) + p_{hyd}(x,t), \tag{53}$$

where the thermodynamic part P_{th} is constant in space and does not appear in the momentum equation, and the hydrodynamic part p_{hyd} is neglected in the gas law. In the low-Mach-number approximation, the terms describing work due to viscous stress, $\boldsymbol{\tau} : \nabla \boldsymbol{v}$, and hydrodynamic pressure in the equation for temperature can be neglected. In this study, only gravitation is considered as the external force $\boldsymbol{f}$. Since hydrodynamic pressure p_{hyd} take several magnitudes smaller than P_{th}, the assumption that the hydrodynamic pressure can be neglected in both equation for temperature and the gas law is in fact appropriate. As a result, the Navier-Stokes equations for reacting flow are formulated for low-Mach-number approximation in the following way:

- Mass conservation of species

$$\frac{\partial \rho Y_i}{\partial t} + \nabla \cdot (\rho Y_i \boldsymbol{v}) = \nabla \cdot (\rho D_i \nabla Y_i) + w_i \qquad (i = 1, 2..., N) \tag{54}$$

- Mass conservation

$$\frac{\partial \rho}{\partial t} + \nabla \cdot (\rho \boldsymbol{v}) = 0 \tag{55}$$

- Momentum conservation

$$\frac{\partial \rho \boldsymbol{v}}{\partial t} + \nabla \cdot (\rho \boldsymbol{v} \otimes \boldsymbol{v}) = -\nabla p_{hyd} + \nabla \cdot \boldsymbol{\tau} + \rho \boldsymbol{g} \tag{56}$$

- Energy equation

$$\rho Cp \left(\frac{\partial T}{\partial t} + \boldsymbol{v} \cdot \nabla T \right) = \frac{\partial P_{th}}{\partial t} + \nabla \cdot (\lambda \nabla T) + \rho \left(\sum_i^N Cp_i D_i \nabla Y_i \right) \cdot \nabla T - \sum_i^N h_i w_i \tag{57}$$

- Thermal state of equation

$$P_{th} = \rho \frac{RT}{M} = \rho RT \sum_{i=1}^{N} \frac{Y_i}{M_i} \tag{58}$$

Here we consider the case where Ω is an open domain. The thermodynamic pressure remains constant in both time and space, independently of the assumptions imposed,

$$P_{th} \equiv const. \tag{59}$$

We then can use the iterative implict scheme to solve numerically the system of these equations in the similar way described as the numerical method for the Boussinesq approximation in the previous section.

4.2 Numerical results

In order to verify the codes, computation of the premixed combustion of hydrogen and bromine was performed. This problem has been investigated by Spalding and Stephenson [8] in which the following four-stage elementary reactions are taken into account:

$$\begin{aligned}
&(1) \qquad Br_2 + M \leftrightarrow 2Br + M \\
&(2) \qquad H_2 + M \leftrightarrow 2H + M \\
&(3) \qquad Br + H_2 \leftrightarrow HBr + H \\
&(4) \qquad H + Br_2 \leftrightarrow HBr + Br
\end{aligned}$$

The schematic of the computational model is shown in Fig. 4.

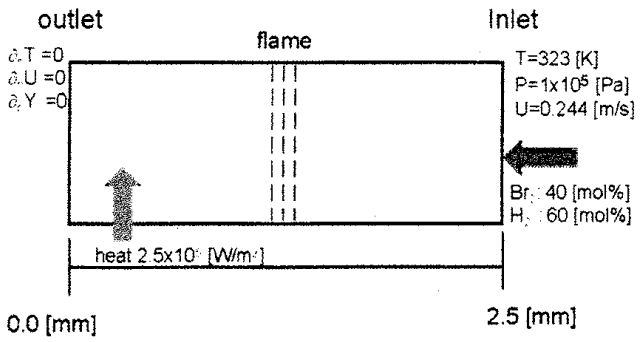

Figure 4: Schematic model of laminar flame propagation of combustion of hydrogen and bromine

4.2.1 Calculation condition

The reaction rate constant for the i-th stage, k_i, is computed by means of Arrhenius' law, as follows:

$$k_i = B_i T^{\alpha_i} exp\left(\frac{-E_i}{RT}\right) \quad [(mol/m^3)^{1-n}s^{-1}], \tag{60}$$

where B_i is the frequency factor $[(mol/m^3)^{1-n}K^{-\alpha_i}s^{-1}]$, E_i means the activation energy $[J/mol]$ α_i denotes the temperature dependent parameter, T stands for the absolute temperature $[K]$, R represents the universal gas constant $[J/mol.K] = 8.314[J/(mol\,K)]$, and n denotes the reaction index $n = a + b$. The Arrhenius parameters used in this study are shown in Table 1 below. The material properties for chemical species are calculated through the following temperature

Reaction	**Forward Reaction**			**Backward Reaction**		
Arrhenius parameters	B_i	α_i	E_i	B_i	α_i	E_i
(1) $Br_2 + M \leftrightarrow 2Br + M$	7.03×10^{11}	-0.5	196700	3.63×10^3	0.0	0
(2) $H_2 + M \leftrightarrow 2H + M$	7.63×10^{13}	-1.0	452100	3.63×10^3	0.0	0
(3) $Br + H_2 \leftrightarrow HBr + H$	3.46×10^4	1.0	69490	9.06×10^5	0.5	7158
(4) $H + Br_2 \leftrightarrow HBr + Br$	6.42×10^6	0.5	4646	6.52×10^4	1.0	178300

Table 1: Chemical reaction parameters

dependent formula.

Diffusion coefficient D**:**

$$D = D_0 \left(\frac{T}{T_{ref}}\right)^{1.67} \tag{61}$$

Thermal conductivity λ**:**

$$\lambda = \lambda_0 \left(\frac{T}{T_{ref}}\right)^{0.67} \tag{62}$$

where $T_{ref} = 323\ [K]$, the parameter D_0 in the equation of the diffusion coefficient and parameter λ_0 in the equation of the thermal conductivity are listed in Table 2 below. The same value of C_p is used for all species as in the paper by Spalding and Stephenson [8], i.e., $C_p = 530.86\ \ [J/(kg\ K)]$.

Species	**Molecular Mass**$[kg/mol]$	**Enthalpy**$[J/mol]$	$D_0\ [m^2/s]$	$\lambda_0\ [W/mK]$
H_2	2.016×10^{-3}	0.0	1.01×10^{-5}	3.34×10^{-2}
Br_2	159.8×10^{-3}	3.09×10^{4}	1.01×10^{-5}	3.34×10^{-2}
HBr	80.908×10^{-3}	-3.66×10^{4}	1.01×10^{-5}	3.34×10^{-2}
H	1.008×10^{-3}	2.18×10^{5}	1.01×10^{-5}	3.34×10^{-2}
Br	79.90×10^{-3}	1.12×10^{5}	1.01×10^{-5}	3.34×10^{-2}

Table 2: Properties of species

4.2.2 Initial and boundary conditions

As initial conditions, the velocity is set to be zero ($u = 0\,[m/s]$), the temperature is set to be $49.85\,^{\circ}C$, the pressure is set to be $1 \times 10^5\,[Pa]$, the mole fraction of bromine is set to be 0.4 ($X_{Br_2} = 0.4$), and the mole fraction of hydrogen is set to be 0.6 ($X_{H_2} = 0.6$) in the whole computational domain. More precisely, the following boundary conditions are used:

On the inlet boundary:

$$u = 0.244\ [m/s],\quad T = 49.85\ [^{\circ}C],\quad p_n = 0,$$
$$X_{Br_2} = 0.4,\quad X_{H_2} = 0.6,\quad X_{HBrn} = 0,\quad X_{Hn} = 0,\quad X_{Brn} = 0.$$

On the outlet boundary:

$$u_n = 0,\quad T_n = 0,\quad p = 1 \times 10^5\ [Pa],$$
$$X_{Br_2n} = 0,\quad X_{H_2n} = 0,\quad X_{HBrn} = 0,\quad X_{Hn} = 0,\quad X_{Brn} = 0.$$

Here subscript "$_n$" denotes the derivative in the normal direction to the boundary.

4.2.3 Computational results

At the beginning of computation, heat source is given nearby outlet as follows.

$$S(x,0) = 2.5 \times 10^{10}\ [W/m^3]\quad x \in [0.75 \times 10^{-4}, 1 \times 10^{-4}]\ [m] \tag{63}$$

As time goes by, the flame surface has propagated toward the center of the computational domain. When the flame reached to the center, the heat source has been removed. After then, the flame propagation has stopped and kept the position. The computation has been made until the temperature and species concentrations reached the steady state. The computed species

concentrations and temperature are shown in Fig. 5. From the right boundary, unburnt gases come into the computational domain, and the flame front is formed around the center of domain. In order that gases come from the inlet boundary with the velocity of 0.244 $[m/s]$, the flame front moves with the relative velocity to the coming gases. Since the mainstream velocity of 0.244 $[m/s]$ is equal to the laminar flame propagation speed on this combustion, the flame propagation stops around center of the domain after the removement of the heat source. It is seen that the radical species, H and Br have the peak values just behind flame front surface. The results taken from Spalding and Stephenson [8] is also shown in Fig. 6. Our result is in good agreement with that of Spalding and Stephenson. Thus, it is confirmed that the results obtained through our numerical scheme are reasonable.

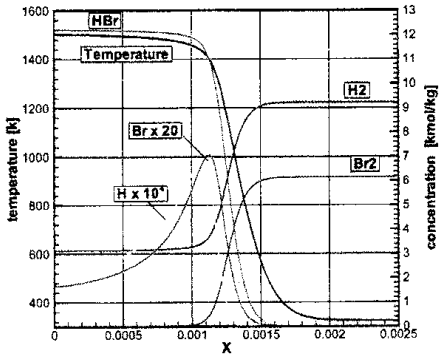

Figure 5: Profiles of computational results of concentration and temperature of the species

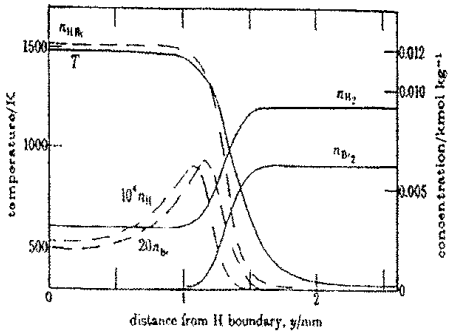

Figure 6: Results cited from Spalding and Stephenson [8]

5 Numerical Simulations with The Aid of Preconditioning Method

It is known that the application of a known numerical method for the compressible Navier-Stokes equations such as Beam-Warming method [2] to low-speed flows does not necessarily provide us with satisfactory results regarding the convergence. This fact implies that numerical simulations become insufficient and the associated computational results turn out to be inaccurate. The numerical difficulties are caused by the circumstances that there are two types of characteristic velocities in the compressible Navier-Stokes system, the convective and sound speeds. Their ratios become large and the so-called stiffness of the system may occur due to the disparity of eigenvalues of the system. In order to overcome this difficulty a preconditioning method is applied to a conventional numerical computation scheme for the compressible Navier-Stoeks equations. The implementation process proposed here have a feature that the dependent variables remain to be unknown conservation variables. Our simulation code is examined through computation of

lid-driven cavity flows at low-Mach numbers, and supersonic channel flows. For Mach numbers below 0.2, the rate of convergence and accuracy of the solver are significantly improved compared to the original compressible-flow solvers. Thus the present approach is useful for the computation of fluid flows for a wide range of Mach numbers.

5.1 Governing Equations

As the governing equations in this study, we employ the two-dimensional Navier-Stokes equations which is written by means of the conservative quantities as the dependent variables in a conservation form. Using a domain $\mathbb{G} \subset \mathbb{R}^2$, we may present a normalized form in a generalized curvilinear coordinate system in the following way:

$$\frac{\partial \mathbf{Q}}{\partial t} + \frac{\partial \mathbf{E}}{\partial \xi} + \frac{\partial \mathbf{F}}{\partial \eta} = \frac{1}{Re}\left[\frac{\partial \mathbf{R}}{\partial \xi} + \frac{\partial \mathbf{S}}{\partial \eta}\right] \quad \text{in } \mathbb{G} \times \mathbb{R}_0^+. \tag{64}$$

Here $t \in \mathbb{R}_0^+$ means time, $\mathbf{Q}$ stands for the vector of conservative dependent variables, and $\mathbf{E}$ and $\mathbf{F}$ represent the convective flux vectors, respectively. $\mathbf{R}$ and $\mathbf{S}$ are the viscous flux vectors, and ξ and η are the streamwise and normal generalized coordinates, respectively. The constant Re is the reference Reynolds number, that is specified later. The vectors $\mathbf{Q}$, $\mathbf{E}$, $\mathbf{F}$, $\mathbf{R}$, and $\mathbf{S}$ are defined as follows:

$$\mathbf{Q} = \frac{1}{J}[\rho, \rho u, \rho v, e]^t, \tag{65}$$

$$\mathbf{E} = \frac{1}{J}\begin{bmatrix} \rho U_\xi \\ \rho u U_\xi + \xi_x p \\ \rho v U_\xi + \xi_y p \\ (e+p) - \xi_t p \end{bmatrix}, \quad \mathbf{F} = \frac{1}{J}\begin{bmatrix} \rho U_\eta \\ \rho u U_\eta + \eta_x p \\ \rho v U_\eta + \eta_y p \\ (e+p) - \eta_t p \end{bmatrix}, \tag{66}$$

$$\mathbf{R} = \frac{1}{J}\begin{bmatrix} 0 \\ \xi_x \tau_{xx} + \xi_y \tau_{xy} \\ \xi_x \tau_{xy} + \xi_y \tau_{yy} \\ \xi_x \beta_x + \xi_y \beta_y \end{bmatrix}, \quad \mathbf{S} = \frac{1}{J}\begin{bmatrix} 0 \\ \eta_x \tau_{xx} + \eta_y \tau_{xy} \\ \eta_x \tau_{xy} + \eta_y \tau_{yy} \\ \eta_x \beta_x + \eta_y \beta_y \end{bmatrix}. \tag{67}$$

Here J represents the Jacobian of coordinate transformation, ρ means the density, u and v are the x- and y-component of the velocity vector, respectively. The parameter e is the total energy per unit volume, U_ξ and U_η are the components of the contravariant velocity vector with respect to ξ and η directions, respectively, which are written as

$$U_\xi = u\xi_x + v\xi_y, \qquad U_\eta = u\eta_x + v\eta_y. \tag{68}$$

The parameter p is the pressure written as

$$p = (\gamma - 1)\left\{e - \frac{1}{2}\rho\left(u^2 + v^2\right)\right\} \tag{69}$$

for perfect gases and τ_{xx}, τ_{xy}, τ_{yy} are components of the viscous stress tensor expressed by Eqs. (70)-(72). The parameters β_x and β_y are defined by Eqs. (73) and (74), respectively.

$$\tau_{xx} = 2\mu\frac{\partial u}{\partial y} - \frac{2}{3}\mu\left(\frac{\partial u}{\partial x} + \frac{\partial v}{\partial y}\right) \tag{70}$$

$$\tau_{xy} = \mu\left(\frac{\partial u}{\partial y} + \frac{\partial v}{\partial y}\right) \tag{71}$$

$$\tau_{yy} = 2\mu\frac{\partial v}{\partial y} - \frac{2}{3}\mu\left(\frac{\partial u}{\partial x} + \frac{\partial v}{\partial y}\right) \tag{72}$$

$$\beta_x = u\tau_{xx} + v\tau_{xy} + \frac{\mu/Pr}{\gamma - 1}\frac{\partial c^2}{\partial x} \tag{73}$$

$$\beta_y = u\tau_{xy} + v\tau_{yy} + \frac{\mu/Pr}{\gamma - 1}\frac{\partial c^2}{\partial y} \tag{74}$$

Moreover, γ denotes the ratio of specific heat, c means the speed of sound, and Pr is the Prandtl number. For perfect gases, $\gamma = 1.4$, $c^2 = \gamma p/\rho$ and $Pr = 0.71$. Since the equations are nondimensionalized using values for the freestream conditions, i.e., the reference pressure p_∞, the reference density ρ_∞, the reference temperature T_∞, the reference velocity $c_\infty/\sqrt{\gamma}$, the reference viscosity μ_∞, and the reference Reynolds number Re is defined as

$$Re = \frac{\rho_\infty c_\infty L}{\mu\sqrt{\gamma}}. \tag{75}$$

It should be noted that the relationship between the freestream Reynolds number Re_∞ and the reference Reynolds number Re is given by

$$Re_\infty = \frac{\rho_\infty u_\infty L}{\mu_\infty} = ReM_\infty\sqrt{\gamma}, \tag{76}$$

where M_∞ is the freestream Mach number which is defined by $M_\infty = u_\infty/c_\infty$.

5.2 Baseline Method without Preconditioning

Before introducing a preconditioning method, a numerical method for compressible flows in terms of implicit approximate factorization scheme [2] are briefly reviewed. We hereafter call this conventional numerical scheme a *baseline* method. Applying the implicit Euler time-marching method to Eq. (64) gives

$$\mathbf{Q}^{n+1} - \mathbf{Q}^n = -\Delta t\left[\frac{\partial \mathbf{E}(\mathbf{Q}^{n+1})}{\partial \xi} + \frac{\partial \mathbf{F}(\mathbf{Q}^{n+1})}{\partial \eta} - Re^{-1}\left\{\frac{\partial \mathbf{R}(\mathbf{Q}^{n+1})}{\partial \xi} + \frac{\partial \mathbf{S}(\mathbf{Q}^{n+1})}{\partial \eta}\right\}\right]. \tag{77}$$

where Δt represents a time step. The flux vectors are linearized using truncated Taylor-series expansions:

$$\begin{aligned}
\mathbf{E}(\mathbf{Q}^{n+1}) &= \mathbf{E}(\mathbf{Q}^n) + \mathbf{A}^n\left(\mathbf{Q}^{n+1} - \mathbf{Q}^n\right) + O[(\Delta t)^2], \\
\mathbf{F}(\mathbf{Q}^{n+1}) &= \mathbf{F}(\mathbf{Q}^n) + \mathbf{B}^n\left(\mathbf{Q}^{n+1} - \mathbf{Q}^n\right) + O[(\Delta t)^2], \\
\mathbf{R}(\mathbf{Q}^{n+1}) &= \mathbf{E}(\mathbf{Q}^n) + \mathbf{K}_\xi^n\left(\mathbf{Q}^{n+1} - \mathbf{Q}^n\right) + O[(\Delta t)^2], \\
\mathbf{S}(\mathbf{Q}^{n+1}) &= \mathbf{F}(\mathbf{Q}^n) + \mathbf{K}_\eta^n\left(\mathbf{Q}^{n+1} - \mathbf{Q}^n\right) + O[(\Delta t)^2],
\end{aligned} \tag{78}$$

where $\mathbf{A}$ and $\mathbf{B}$ are inviscid Jacobian matrices in the ξ and η directions which are given by

$$\mathbf{A}^n = \left(\frac{\partial \mathbf{E}(\mathbf{Q}^n)}{\partial \mathbf{Q^n}}\right), \quad \mathbf{B}^n = \left(\frac{\partial \mathbf{F}(\mathbf{Q}^n)}{\partial \mathbf{Q^n}}\right), \tag{79}$$

respectively. Also, $\mathbf{K}_\xi$ and $\mathbf{K}_\eta$ are viscous Jacobian matrices in the ξ and η directions which are given by

$$\mathbf{K}_\xi^n = \left(\frac{\partial \mathbf{R}(\mathbf{Q}^n)}{\partial \mathbf{Q^n}}\right), \quad \mathbf{K}_\eta^n = \left(\frac{\partial \mathbf{S}(\mathbf{Q}^n)}{\partial \mathbf{Q^n}}\right), \tag{80}$$

respectively. Substituting Eq. (78) and into Eq. (77), we obtain

$$\left[\mathbf{I} + \triangle t\frac{\partial \mathbf{A}^n}{\partial \xi} + \triangle t\frac{\partial \mathbf{B}^n}{\partial \eta} - \triangle t\frac{1}{Re}\frac{\partial \mathbf{K}_\xi^n}{\partial \xi} - \triangle t\frac{1}{Re}\frac{\partial \mathbf{K}_\eta^n}{\partial \eta}\right]\triangle \mathbf{Q}^n = \mathbf{RHS}^n, \tag{81}$$

where

$$\triangle \mathbf{Q}^n = \mathbf{Q}^{n+1} - \mathbf{Q}^n, \tag{82}$$

and

$$\mathbf{RHS}^n = -\triangle t\left[\frac{\partial \mathbf{E}(\mathbf{Q}^n)}{\partial \xi} + \frac{\partial \mathbf{F}(\mathbf{Q}^n)}{\partial \eta} - Re^{-1}\left\{\frac{\partial \mathbf{R}(\mathbf{Q}^n)}{\partial \xi} + \frac{\partial \mathbf{S}(\mathbf{Q}^n)}{\partial \eta}\right\}\right]. \tag{83}$$

Here, $\mathbf{I}$ means the unit matrix in the space $\mathbb{R}^4 \times \mathbb{R}^4$. This difference formula is of the so-called delta form. This form has an advantage of yielding steady-state solutions (independent of the time step) for problems that possess steady-state solutions. Applying an implicit approximate factored (IAF) scheme due to Beam and Warming [2] and appropriate spatial discretization to Eq. (81), we obtain

$$\left[\mathbf{I} + \triangle t\delta_\xi \mathbf{A}^n - \triangle t Re^{-1}\delta_\xi {\mathbf{K}_\xi}^n\right]\left[\mathbf{I} + \triangle t\delta_\eta \mathbf{B}^n - \triangle t Re^{-1}\delta_\eta {\mathbf{K}_\eta}^n\right]\triangle \mathbf{Q}^n = \mathbf{rhs}^n, \tag{84}$$

where

$$\mathbf{rhs}^n = -\triangle t\left[\delta_\xi \mathbf{E}(\mathbf{Q}^n) + \delta_\eta \mathbf{F}(\mathbf{Q}^n) - Re^{-1}\left\{\delta_\xi \mathbf{R}(\mathbf{Q}^n) + \delta_\eta \mathbf{S}(\mathbf{Q}^n)\right\}\right]. \tag{85}$$

Here, the symbol δ denotes the operator for spatial discretization. The application of the three-point finite difference scheme to the operator for spatial discretization of Eq. (84) gives a 4×4 bock tridiagonal matrix for each factor on the left-hand side of the equation. Therefore, we can solve $\triangle \mathbf{Q}^n$ by applying the inverse matrices of the 4×4-block tridiagonal matrix in the ξ and η directions. Thus, the solution $\mathbf{Q}^{n+1}$ is obtained from $\mathbf{Q}^{n+1} = \mathbf{Q}^n + \triangle \mathbf{Q}^n$.

5.3 Local Preconditioning

The eigenvalues of the inviscid Jacobian matrices $\mathbf{A}$ and $\mathbf{B}$ are U_ξ, U_ξ, $U_\xi \pm c\sqrt{{\xi_x}^2 + {\xi_y}^2}$ and U_η, U_η, $U_\eta \pm c\sqrt{{\xi_x}^2 + {\xi_y}^2}$, respectively. Since the flow asymptotically approaches an incompressible flow as $c \to \infty$, these eigenvalues are of widely differing magnitudes and then the system becomes stiff. Hence the local preconditioning matrix $\mathbf{\Gamma}$ is introduced as follows:

$$\mathbf{\Gamma}\frac{\partial \mathbf{Q}}{\partial t} + \frac{\partial \mathbf{E}}{\partial \xi} + \frac{\partial \mathbf{F}}{\partial \eta} = \frac{1}{Re}\left[\frac{\partial \mathbf{R}}{\partial \xi} + \frac{\partial \mathbf{S}}{\partial \eta}\right]. \tag{86}$$

Although the destruction of the time derivative is made in the above equation by multiplying the preconditioning matrix $\mathbf{\Gamma}$, it seems that this does not affect the steady-state solution. Multiplying Eq. (86) by the matrix $\mathbf{\Gamma}^{-1}$ from the left gives

$$\frac{\partial \mathbf{Q}}{\partial t} + \mathbf{\Gamma}^{-1}\mathbf{A}\frac{\partial \mathbf{Q}}{\partial \xi} + \mathbf{\Gamma}^{-1}\mathbf{B}\frac{\partial \mathbf{Q}}{\partial \eta} = \frac{1}{Re}\mathbf{\Gamma}^{-1}\left[\frac{\partial \mathbf{R}}{\partial \xi} + \frac{\partial \mathbf{S}}{\partial \eta}\right]. \tag{87}$$

It is seen that the preconditioned inviscid Jacobian matrices become $\mathbf{\Gamma}^{-1}\mathbf{A}$ and $\mathbf{\Gamma}^{-1}\mathbf{B}$. An appropriate choice of the preconditioning matrix $\mathbf{\Gamma}$ can make the quotient of the maximum and minimum eigenvalues close to one.

5.3.1 Preconditioning for Euler equations

Before introducing the preconditioning matrix $\mathbf{\Gamma}$ for the Navier-Stokes equations, we consider a new form of the Euler equations with respect to the so-called *symmetry variables* for the sake of convenience. For symmetry variables, we have

$$\partial \hat{\mathbf{Q}} = J^{-1}\left[\frac{1}{\rho c}\partial p,\ \partial u,\ \partial v,\ \partial s\right]^t, \tag{88}$$

and the Euler equations can be written as

$$\frac{\partial \hat{\mathbf{Q}}}{\partial t} + \hat{\mathbf{A}}\frac{\partial \hat{\mathbf{Q}}}{\partial \xi} + \hat{\mathbf{B}}\frac{\partial \hat{\mathbf{Q}}}{\partial \eta} = 0, \tag{89}$$

where s means the entropy defined by $\partial s = \partial p - c^2 \partial \rho$. The matrices $\hat{\mathbf{A}}$ and $\hat{\mathbf{B}}$ are the flux Jacobian matrices in the ξ and η directions, respectively. which are defined by

$$\hat{\mathbf{A}} = \begin{bmatrix} U_\xi & \xi_x c & \xi_y c & 0 \\ \xi_x c & U_\xi & 0 & 0 \\ \xi_y c & 0 & U_\xi & 0 \\ 0 & 0 & 0 & U_\xi \end{bmatrix}, \quad \hat{\mathbf{B}} = \begin{bmatrix} U_\eta & \eta_x c & \eta_y c & 0 \\ \eta_x c & U_\eta & 0 & 0 \\ \eta_y c & 0 & U_\eta & 0 \\ 0 & 0 & 0 & U_\eta \end{bmatrix}. \tag{90}$$

We then introduce a preconditioning matrix to the Euler equations.

$$\hat{\mathbf{\Gamma}}\frac{\partial \hat{\mathbf{Q}}}{\partial t} + \hat{\mathbf{A}}\frac{\partial \hat{\mathbf{Q}}}{\partial \xi} + \hat{\mathbf{B}}\frac{\partial \hat{\mathbf{Q}}}{\partial \eta} = 0. \tag{91}$$

Then we have

$$\frac{\partial \hat{\mathbf{Q}}}{\partial t} + \hat{\mathbf{\Gamma}}^{-1}\hat{\mathbf{A}}\frac{\partial \hat{\mathbf{Q}}}{\partial \xi} + \hat{\mathbf{\Gamma}}^{-1}\hat{\mathbf{B}}\frac{\partial \hat{\mathbf{Q}}}{\partial \eta} = 0. \tag{92}$$

The preconditioning matrix in terms of the symmetry variables proposed by Weiss and Smith [10] is of a simple form such as

$$\hat{\mathbf{\Gamma}} = \begin{bmatrix} \frac{1}{\epsilon} & 0 & 0 & 0 \\ 0 & 1 & 0 & 0 \\ 0 & 0 & 1 & 0 \\ 0 & 0 & 0 & 1 \end{bmatrix}, \quad \hat{\mathbf{\Gamma}}^{-1} = \begin{bmatrix} \epsilon & 0 & 0 & 0 \\ 0 & 1 & 0 & 0 \\ 0 & 0 & 1 & 0 \\ 0 & 0 & 0 & 1 \end{bmatrix}, \tag{93}$$

where the element ϵ may be taken as

$$\epsilon = min\left[1, max\left(M^2, \phi M_\infty^2\right)\right]. \tag{94}$$

Here, M is the local Mach number specified by means of local variables, and M_∞ is the freestream Mach number. The parameter ϕ is the coefficient which is multiplied the freestream Mach number M_∞ to designate the lower limit of ϵ to avoid the case where $\epsilon = 0$ at $M = 0$, and thus ϵ must satisfy $0 < \epsilon < 1$.

5.4 Eigenvalues of $\hat{\Gamma}^{-1}\hat{\mathbf{A}}$ and $\hat{\Gamma}^{-1}\hat{\mathbf{B}}$

We see that the eigenvalues of the preconditioned flux Jacobian matrices $\hat{\Gamma}^{-1}\hat{\mathbf{A}}$ and $\hat{\Gamma}^{-1}\hat{\mathbf{B}}$ are the same as the original ones, as $\epsilon \to 1$.

Since the following discussions on $\hat{\Gamma}^{-1}\hat{\mathbf{A}}$ and $\hat{\Gamma}^{-1}\hat{\mathbf{B}}$ can be made in the similar scenario, we consider $\hat{\Gamma}^{-1}\hat{\mathbf{A}}$ only. The diagonalized matrix $\mathbf{\Lambda}_{\xi,\Gamma}$ with the eigenvalues of the Jacobian matrix of $\hat{\Gamma}^{-1}\hat{\mathbf{A}}$ is given by

$$\mathbf{\Lambda}_{\xi,\Gamma} = \begin{bmatrix} U_\xi & 0 & 0 & 0 \\ 0 & U_\xi & 0 & 0 \\ 0 & 0 & \lambda_{\xi,+} & 0 \\ 0 & 0 & 0 & \lambda_{\xi,-} \end{bmatrix}, \tag{95}$$

where U_ξ is the component of the contravariant velocity vector in the ξ direction and $\lambda_{\xi,\pm}$ are easily found as

$$\lambda_{\xi,\pm} = \frac{1}{2}(1+\epsilon)U_\xi \pm \frac{1}{2}\sqrt{(\epsilon-1)^2 {U_\xi}^2 + 4\epsilon\left({\xi_x}^2 + {\xi_y}^2\right)c^2}. \tag{96}$$

We see that as $\epsilon \to 0$, all eigenvalues of the preconditioned flux Jacobian matrices $\hat{\Gamma}^{-1}\hat{\mathbf{A}}$ become U_ξ.

6 Preconditioning Method for the Navier-Stokes Equations

The symmetry variables and the conservative variables can be related with the following transfer matrices,

$$\mathbf{M} = \frac{\partial \mathbf{Q}}{\partial \hat{\mathbf{Q}}}, \qquad \mathbf{M}^{-1} = \frac{\partial \hat{Q}}{\partial Q}. \tag{97}$$

The following important relations allow us to apply the preconditioning for the symmetry variables to the Navier-Stokes equations in terms of conservative variables as follows.

$$\mathbf{\Gamma} = \mathbf{M}\hat{\mathbf{\Gamma}}\mathbf{M}^{-1} \tag{98}$$

$$\mathbf{A} = \mathbf{M}\hat{\mathbf{A}}\mathbf{M}^{-1} \tag{99}$$

$$\mathbf{B} = \mathbf{M}\hat{\mathbf{B}}\mathbf{M}^{-1}. \tag{100}$$

Thus,

$$\mathbf{M}\hat{\mathbf{\Gamma}}\mathbf{M}^{-1}\frac{\partial \mathbf{Q}}{\partial t} + \frac{\partial \mathbf{E}}{\partial \xi} + \frac{\partial \mathbf{F}}{\partial \eta} = \frac{1}{Re}\left[\frac{\partial \mathbf{R}}{\partial \xi} + \frac{\partial \mathbf{S}}{\partial \eta}\right] \tag{101}$$

Equations.(98), (99), and (100) together imply

$$\begin{aligned} \mathbf{M}\hat{\mathbf{\Gamma}}^{-1}\hat{\mathbf{A}}M^{-1} &= \mathbf{\Gamma}^{-1}\mathbf{A} \\ \mathbf{M}\hat{\mathbf{\Gamma}}^{-1}\hat{\mathbf{B}}M^{-1} &= \mathbf{\Gamma}^{-1}\mathbf{B}. \end{aligned} \tag{102}$$

It is seen from Eq. (102) that $\hat{\mathbf{\Gamma}}^{-1}\hat{\mathbf{A}}$ and $\mathbf{\Gamma}^{-1}\mathbf{A}$ have the same eigenvalues, and that $\hat{\mathbf{\Gamma}}^{-1}\hat{\mathbf{B}}$ and $\mathbf{\Gamma}^{-1}\mathbf{B}$ have the same eigenvalues as well.

7 Validation of Codes

For the validation of low speed flow condition, the lid-driven flow in square cavity shown in Figs. 7(a) has been simulated for $Re = 10,000$. For all walls, an adiabatic condition is imposed on the temperature. The non-slip velocity condition is applied to the bottom, right and left walls. The top wall is assumed to move with the uniform velocity of $M = 0.01$. The size of cavity is set so that the Reynolds number is equal to the given conditions. As initial conditions, the pressure is set to be 0.1MPa, and the temperature is set to be $300K$. The numerical results are compared with Ghia's numerical results [4] and Nallasamy's experimental data [4]. These results have been cited for validation of many CFD codes. For the validation of high speed flow conditions, the supersonic channel flow has been computed as shown in Fig. 7(b). A channel with a compression corner and an expansion corner located at the lower and upper straight surfaces are considered. The obtained results have been compared with the exact solutions of one-dimensional Euler equations. Supersonic flow with Mach number 2.0 enters the channel from the left side.

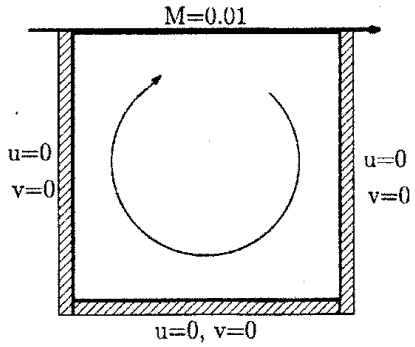

(a) Lid-driven square cavity flow

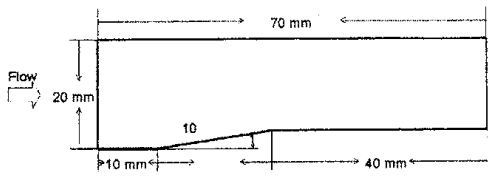

(b) Super-sonic channel flow

Figure 7: Schematics of test case problems

Figure 8 shows the numerical results of flows in square cavity for the Reynolds numbers $Re = 10,000$. The numerical contours of stream function are depicted in Fig. 8(a), and the numerical velocity profiles for vertical and horizontal lines passing through the geometric center of the cavity are shown in Fig. 8(b). In this figure, the numerical u-velocity along vertical line and v-velocity along horizontal line through geometric center are shown with the numerical results of

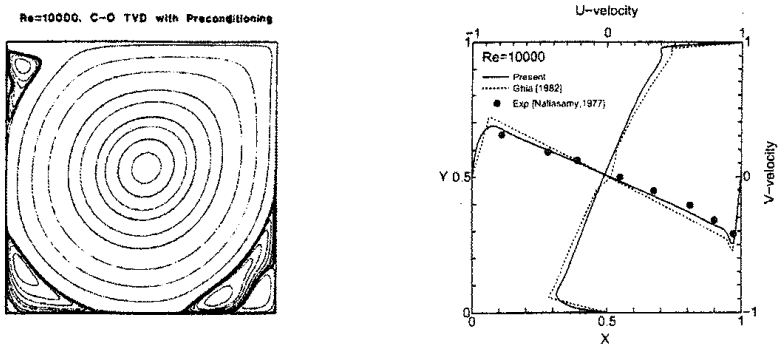

(a) streamline (b) velocity profile

Figure 8: Cavity flows, $Re = 10,000$, $M_{Lid} = 0.01$

Ghia et al. and the experimental data of Nallasamy [4]. Our results agree well with the results of Ghia et al. and Nallasamy.

In Fig. 9, the numerical density contours of the supersonic channel flow is shown. The density contours illustrate the formation of oblique shock, expansion wave, and their reflection and interaction. In Fig. 10, the numerical density and pressure along bottom line are compared with the analytical solutions of the one-dimensional Euler equations. It is seen that the numerical results are in good agreement with the data used for comparisons.

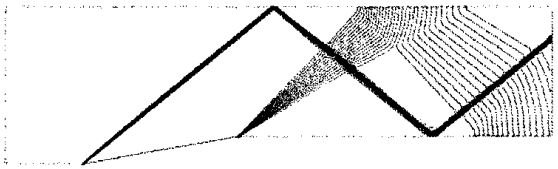

Figure 9: Density contours in supersonic channel at $M_{in} = 2.0$

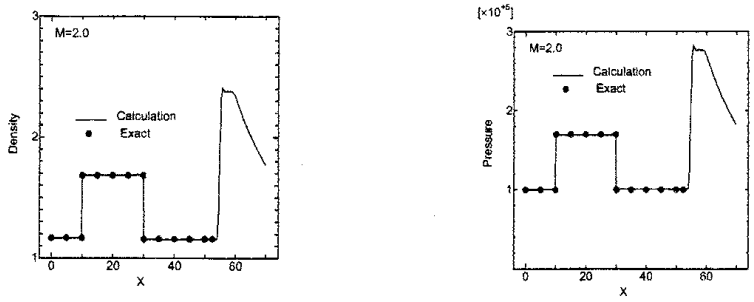

(a) density (a) pressure

Figure 10: comparison with exact solution

8 Conclusions

The mathematical model describing the fluid flow motions is the Navier-Stokes equations. However, it is difficult to solve in a consistent way the equations of this system through the state-of-the-art numerical methods in a wide range of variation of density. Furthermore, the environmental fluid dynamics necessitates to dealing with multidisciplinary phenomena such as thermochemical science, chemical reactions, phase transitions, and so on. Obviously, it is necessary to formulate adequate mathematical models which specifically describe important phenomena based on a complete mathematical model as well as appropriate constitutive equations for such physical phenomena. In this paper, numerical methods for environmental fluid dynamics are classified into three types of mathematical models in terms of rate of the density variation and new numerical methods for the approximate equations are discussed. From the point of view of practical numerical computation, implicit time marching schemes are particularly of importance because of its stability and robustness. We focus our attention on the implicit iterative schemes that is much more economical in computation than known schemes but also retains most of the stability and accuracy of the fully implicit scheme.

References

[1] R. B. Bird, W. E. Stewart and E. N. Lighfoot, *Transport Phenomena*, John Wiley & Sons, Inc., 1960.

[2] R. M. Beam and R. F. Warming, An implicit finite-difference algorithm for hyperbolic system in conservation law form, *Journal of Computational Physics*, **22**, (1976), pp. 87–109.

[3] S. R. Chakravarthy and S. Osher, A new class of high accuracy TVD scheme for hyperbolic conservation laws, AIAA Paper 85-0363, (1985).

[4] U. Ghia, K. N. Ghia and C. T. Shin, High-Re solutions for incompressible flow using the Navier-Stokes equations and a multi-grid method, *Journal of Computational Physics*, **48**, (1982), pp. 387–411.

[5] F. H. Harlow and J. E. Welch, Numerical calculation of time-dependent viscous incompressible flow of fluid with free surface, *The Physics of Fluids*, **8** (12), (1965), pp. 2182–2189.

[6] A. Harten, On a class of high resolution Total-Variation-Stable finite-difference schemes, *SIAM Journal of Numerical Analysis*, **21** (1), (1984), pp. 1–12.

[7] A. Majda, Compressible fluid flow and systems of conservation laws in several space variable, Springer, New York, 1984.

[8] D. B. Spalding and P. L. Stephenson, Laminar flame propagation in hydrogen+bromine mixtures, *Proceedings of the Royal Socciety of London*, **A324**, 315, 1971.

[9] B. van Leer, Toward the ultimate conservative difference scheme. 4, A new approach to numerical convection, *Journal of Computational Physics*, **23**, (1977), pp. 276–299.

[10] J. M. Weiss and W. A. Smith, Preconditioning applied to variable and constant density flows, *AIAA Journal*, **33** (11), (1995), pp. 2050–2057.

[11] C. R. Wilke, *Journal of Chemical Physics*, **18**, 517, 1950.